

Cite this article as: Wang Meihan, Chen Yun, Wang Guanjie, et al. Electrochromic Properties of Nano-columnar Porous $\text{WO}_{3-x}/\text{TiO}_2$ Thin Films[J]. Rare Metal Materials and Engineering, 2022, 51(08): 2732-2738.

ARTICLE

Electrochromic Properties of Nano-columnar Porous $\text{WO}_{3-x}/\text{TiO}_2$ Thin Films

Wang Meihan¹, Chen Yun¹, Wang Guanjie¹, Lei Hao², Sun Lixian³, Xu Fen³, Zhang Jun¹

¹School of Mechanical Engineering, Shenyang University, Shenyang 110044, China; ²Aluminum Valley Industrial Technology Institute, Zouping 256200, China; ³Guangxi Key Laboratory of Information Materials, Guilin University of Electronic Technology, Guilin 541004, China

Abstract: Tungsten oxide (WO_{3-x}) thin films were fabricated by reactive magnetron sputtering at glancing angle $\alpha=0^\circ$ or $\alpha=80^\circ$, and then titanium oxide (TiO_2) was deposited on it. X-ray diffraction (XRD), field emission scanning electron microscopy (FE-SEM) and X-ray photoelectron spectroscopy (XPS) were employed to characterize the crystal structure, surface/cross-section morphologies, and surface chemical composition of the $\text{WO}_{3-x}/\text{TiO}_2$ thin films. Electrochromic properties of the $\text{WO}_{3-x}/\text{TiO}_2$ thin films were measured by electrochemical workstation in three-electrode system with 1 mol/L LiClO_4/PC solution and UV-Vis spectrophotometer. Results reveal that the $\text{WO}_{3-x}/\text{TiO}_2$ thin films present totally amorphous structure independent on glancing angles. As the glancing angle is kept at 80° , the nano-columnar porous thin film is obtained. Substoichiometric tungsten oxide (WO_{3-x}) and stoichiometric titanium oxide (TiO_2) are confirmed by XPS spectra of W 4f and Ti 2p, respectively. Compared with the dense thin film, the nano-columnar porous film needs a lower driving potential and presents faster response. The charge capacity of the nano-columnar porous film is calculated to be 83.78 mC, which is over twice higher than 30.83 mC of the dense film. The intercalation and deintercalation ion diffusion rates are determined to be $D_{\text{in}}=5.69\times 10^{-10}\text{ cm}^2\cdot\text{s}^{-1}$ and $D_{\text{de}}=5.08\times 10^{-10}\text{ cm}^2\cdot\text{s}^{-1}$ at the applied potential $\pm 1.2\text{ V}$, respectively. The electrochromic cycle of the nano-columnar porous $\text{WO}_{3-x}/\text{TiO}_2$ thin film is more stable than that of pure WO_3 thin film. The optical density variation (ΔOD) of the nano-columnar porous thin film is larger than that of the dense thin film due to the larger optical modulation amplitude in the whole visible wavelengths.

Key words: $\text{WO}_{3-x}/\text{TiO}_2$ thin films; nano-columnar; glancing angle; magnetron sputtering; electrochromic properties

Tungsten oxides (WO_{3-x}) as important inorganic chromogenic materials have been intensively investigated due to their excellent electrochromic performances^[1-4]. However, the properties of pure WO_{3-x} thin film such as reversibility, stability and optical modulation fall short of the requirements for practical application in smart windows. Since these drawbacks are difficult to overcome for the pure WO_{3-x} , many attempts have been made to solve them by doping or mixing with other transition metal oxide^[5], most notably titanium oxide (TiO_2). Much effort has been dedicated to understand the effects of TiO_2 on the improvement of cyclic stability of WO_{3-x} thin films^[6-9]. Although the $\text{WO}_{3-x}/\text{TiO}_2$ thin films exhibit good electrochromic lifetime, little enhancement of the coloration efficiency is achieved due to the limitation of charge transport kinetics as well as ion migration at the

interfacial and internal of $\text{WO}_{3-x}/\text{TiO}_2$ thin films.

One extensively adopted way to improve coloration efficiency is to tailor the morphology of the $\text{WO}_{3-x}/\text{TiO}_2$ thin films to design spacious channels, which facilitate charge or ion injection into and transport within the films. $\text{WO}_{3-x}/\text{TiO}_2$ thin films with nano-structure offer an extremely large specific surface area and short charge transport distance, which facilitate the interaction between electrolyte and thin films, thereby resulting in remarkable enhancement of electrochemical activities^[10]. Therefore, nano-technology makes it possible to realize fast switching time, high coloration efficiency, and good stability of $\text{WO}_{3-x}/\text{TiO}_2$ thin films.

There are various chemical methods to fabricate nano-structured $\text{WO}_{3-x}/\text{TiO}_2$ thin films, including anodic

Received date: August 12, 2021

Foundation item: Program for Innovation Talents in University of Liaoning Province (LR2019044); Natural Science Foundation of Liaoning Province of China (2019-ZD-0540); Program for Young and Middle-aged Innovation Talents in Science and Technologies of Shenyang (RC190359); Project of Guangxi Key Laboratory of Information Materials (Guilin University of Electronic Technology), China (191007-K)

Corresponding author: Wang Meihan, Ph. D., Professor, Shenyang University, Shenyang 110044, P. R. China, E-mail: mhwang@syu.edu.cn

Copyright © 2022, Northwest Institute for Nonferrous Metal Research. Published by Science Press. All rights reserved.

oxidization^[11], hydrothermal method^[12], sol-gel^[13] etc. However, those methods often require multiple steps and are seriously reliant on chemical processes. Various nano-size, random distribution and irregular orientation result in a poor electrochromic reproducibility of thin films. Glancing angle magnetron sputtering as one of physical vapor deposition method provides a high degree of precise control over the size, distribution and morphology of nano-structured thin films through optimizing deposition parameters, which also creates uniform results^[14,15]. Our previous study using this method to deposit pure WO_{3-x} thin films has proved that it is an effective way to deposit nano-columnar porous thin films^[16,17].

Therefore, nano-columnar porous WO_{3-x}/TiO₂ thin films were deposited by glancing angle magnetron sputtering. The combination of electrochemical properties and light modulation ability was applied to demonstrate the enhanced electrochromic performance of nano-columnar porous WO_{3-x}/TiO₂ thin film, benchmarked against dense WO_{3-x}/TiO₂ thin film fabricated by planar magnetron sputtering.

1 Experiment

1.1 Deposition of WO_{3-x}/TiO₂ thin films

Sn-doped In₂O₃ (ITO) glasses (25 mm×50 mm, sheet resistance<10 Ω/sq, transmittance≥83%) and single crystal silicon wafers (5 mm×20 mm) were chosen as substrates. They were separately cleaned with acetone, deionized water and ethanol for 15 min by ultrasonic wave. Firstly, metal tungsten (W) target ($\Phi = 100$ mm, purity≥99.95%) was employed to deposit pure WO_{3-x} thin films by direct-current reactive magnetron sputtering. The substrates were adjusted to 10 cm far from the target. The sample holder fixed with substrates was tilted at the glancing angle $\alpha = 0^\circ$ or $\alpha = 80^\circ$ during the sputtering deposition. The background pressure of the sputtering chamber was evacuated less than 4.0×10^{-3} Pa using a turbo-molecular pump. High purity argon (99.99%) and oxygen (99.99%) were released into the sputtering chamber at gas flow rates of 26 and 16 mL/min, respectively. The sputtering power was kept at 100 W and sputtering gas pressure was 0.5 Pa. TiO₂ was reactively deposited for 5 min on WO₃/ITO glasses using metal titanium target ($\Phi = 100$ mm, purity≥99.95%) by the same method. The sputtering deposition was carried out at a gas pressure of 0.8 Pa and the sputtering power was maintained at 50 W. Other deposition conditions are the same as those for WO₃ thin films. For each deposition, the WO_{3-x}/TiO₂ film thickness was controlled at about 400 nm.

1.2 Characterization of WO_{3-x}/TiO₂ thin films

The crystal structure of the WO_{3-x}/TiO₂ thin films was confirmed by Rigaku XRD (RINT 2500) with a graphite-monochromated Cu K α radiation. A line-shaped X-ray source was operated at 40 kV and 300 mA. The data were collected in the range of $10^\circ \sim 60^\circ$ with an interval of 0.01° and a scanning speed of $2^\circ \cdot \text{min}^{-1}$.

The surface and cross-section images of WO_{3-x}/TiO₂ thin films were observed using a Hitachi FE-SEM (S-4800) with a

25 kV operation voltage.

The binding energies of W 4f, Ti 2p and O 1s referenced to the C 1s value of 285.0 eV were determined by XPS using a Thermo VG-ESCALAB250 surface analysis system and monochromator Al K α radiation as excitation source. Mild surface cleaning was carried out previously for surface analysis with Ar⁺ sputtering for 60 s.

1.3 Testing of electrochromic properties of WO_{3-x}/TiO₂ thin films

For electrochromic measurements, the WO_{3-x}/TiO₂ thin films as the working electrode were placed into a three-electrode cell filled with $1 \text{ mol} \cdot \text{L}^{-1}$ LiHClO₄/propylene carbonate (PC) electrolyte. The counter and reference electrodes were Pt gauze and saturation Hg/HgO, respectively. Electrochemical workstation (Autolab A25328) was used to control the cyclic voltammetry (CV) measurements and colored/bleached tests at room temperature. Charge storage capacity and ion intercalation/deintercalation diffusion rates were determined from CV curves.

For the optical properties, the transmittance difference between the colored/bleached states was collected by PerkinElmer UV-vis spectrophotometer (Lambda 750) in visible wavelengths.

2 Results and Discussion

The crystal structure, microstructure and surface chemical composition of WO_{3-x}/TiO₂ thin films influence the electrochemical properties and colorization efficiency to a great extent. Therefore, various characterization techniques were used to reveal the structural and surface chemical properties of the WO_{3-x}/TiO₂ thin films deposited at glancing angle $\alpha = 0^\circ$ or $\alpha = 80^\circ$.

2.1 Thin films structure and surface chemical composition

Fig. 1 shows XRD patterns of the WO_{3-x}/TiO₂ thin films deposited at glancing angles $\alpha = 0^\circ$ and $\alpha = 80^\circ$. No sharp peaks except for a broad and diffuse peak are detected in the 2θ range of $20.0^\circ \sim 27.5^\circ$, indicating a totally amorphous structure. The XRD results suggest that glancing angles do not affect the crystallinity of the WO_{3-x}/TiO₂ thin films due to the films deposited at room temperature.

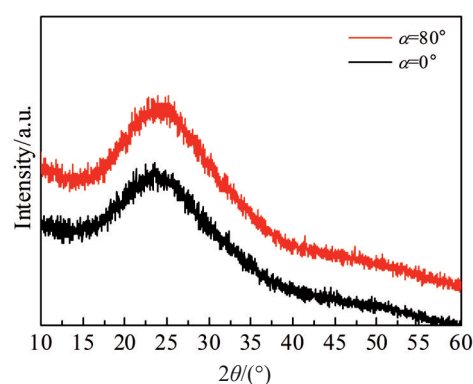


Fig.1 XRD patterns of WO_{3-x}/TiO₂ thin films deposited at glancing angles $\alpha = 0^\circ$ and $\alpha = 80^\circ$

The surface morphology of the $\text{WO}_{3-x}/\text{TiO}_2$ thin film fabricated at glancing angle $\alpha=0^\circ$ is uniform and flat (Fig. 2a). The thin film is extremely dense, observed from the cross-section image (Fig. 2b). In contrast, the surface morphology is found to be rough with remarkable nano-pores (Fig. 2c) and the cross-section image presents columnar structure (Fig. 2d) for the film deposited at $\alpha=80^\circ$, which are ascribed to the self-shadowing effect during the glancing angle magnetron sputtering deposition. Glancing angle deposition is a technique to engineer the columnar structure of thin films at the nano- and micro-scale. One of the advantages of this technique is the possibility of obtaining highly porous thin films that exhibit high aspect ratios of surface area to volume^[18]. Barranco et al^[19] demonstrated that there are three important factors influencing the thin film growth process during glancing angle deposition, i. e. shadowing effect, surface diffusion and internal diffusion. Among them, the shadowing effect plays the most crucial role. The initial nucleation sites and the incoming flux of deposited material are important for the formation of the columnar porous structure in glancing angle

deposition. While the kinetic energy of colliding particles accelerating the surface and internal diffusion tends to smooth the surface and suppress the shadowing effect. The competition of three factors results in the formation of various nano-structured porous thin films. Charles et al^[20] also attributed the formation of the nanostructure to shadowing effect and limited surface diffusion. In this work, the $\text{WO}_{3-x}/\text{TiO}_2$ thin film prepared at glancing angle $\alpha=80^\circ$ exhibits a clear inclined columnar structure. It is mainly ascribed to the shadowing effect at the atomic scale too, which prevails over the surface diffusion of ad-atoms due to the deposition at room temperature.

Signals of elements W (29.2~42.3 eV), Ti (454.6~467.0 eV), and O (527.8~533.4 eV) appear on the XPS survey scan spectra of $\text{WO}_{3-x}/\text{TiO}_2$ thin film deposited at glancing angles of 80° . The high-resolution XPS spectra of W 4f, Ti 2p and O 1s are shown in Fig. 3. W 4f is characterized by two pronounced spin-orbit peaks at lower binding energy 34.5 eV (W 4f_{7/2}) and higher binding energy 37.1 eV (W 4f_{5/2}). These values are lower than that reported for typical of the W⁶⁺ state, which

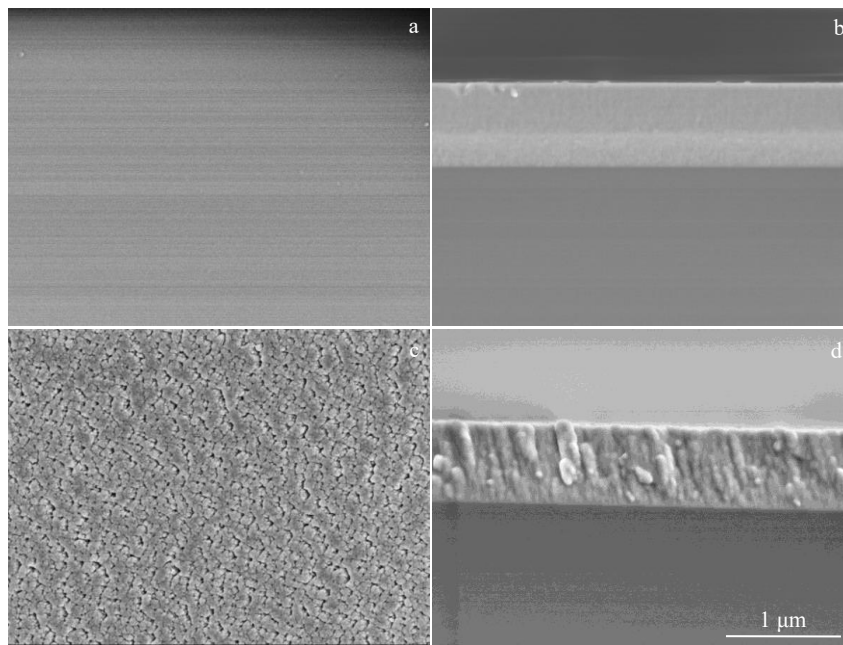


Fig.2 SEM images of $\text{WO}_{3-x}/\text{TiO}_2$ thin films deposited at two glancing angles: (a, b) $\alpha=0^\circ$ and (c, d) $\alpha=80^\circ$

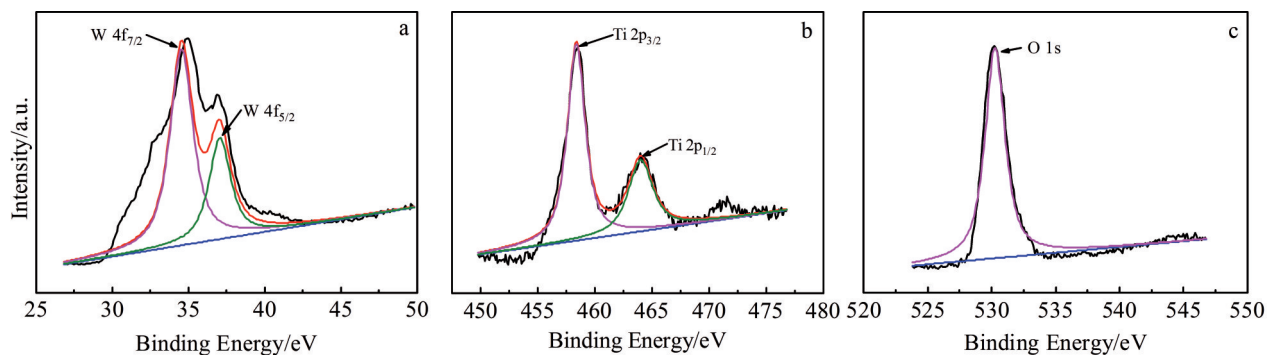


Fig.3 XPS spectra of nano-columnar porous $\text{WO}_{3-x}/\text{TiO}_2$ thin film deposited at glancing angle $\alpha=80^\circ$: (a) W 4f, (b) Ti 2p, and (c) O 1s

indicates sub-stoichiometric WO_{3-x} ^[21]. The corresponding binding energies for Ti 2p_{1/2} and Ti 2p_{3/2} are located at 464.1 and 458.4 eV, respectively, which are comparable with reported values for stoichiometric TiO_2 . Furthermore, the spin-orbit splitting of the Ti 2p doublet is approximately 5.7 eV, indicating that Ti exists in its highest oxidation state^[22]. A single component centered at 530.2 eV is ascribed to the O 1s peak. The peak position shifts to lower binding energy due to lattice oxygen bonding with both W and Ti. The surface concentration atomic ratio of Ti/W is determined to be 1.07.

2.2 Thin films electrochromic properties

Electrochromic performances of the $\text{WO}_{3-x}/\text{TiO}_2$ thin films are determined by their microstructure. Therefore, an endeavoring to relate specific structure with their electrochromic performance is needed. Fig. 4 is the cyclic voltammogram (CV) curves of $\text{WO}_{3-x}/\text{TiO}_2$ thin film deposited at glancing angle of 0° or 80° at the scan rate of 50 $\text{mV}\cdot\text{s}^{-1}$ under different applied potentials.

In CV curves, a cathodic peak, indicating proton insertion into the lattice, appears in the negative potential, whereas the anodic peak, suggesting the oxidization of colored material to the original metal oxide, appears in the positive potential. No anodic peak appears at the applied potential less than 1.0 V for the dense thin film. The peak current increases gradually with the potential, indicating that the potential higher than 1.0 V can drive the colorization. Compared with the dense thin film, an obvious anodic peak (around 0.14 V vs Hg/HgO) appears at the applied potential ± 0.8 V for the nano-columnar porous thin film. In addition, both cathodic peak current values or anodic peak current values at the same driving potential are distinctly higher than those of the dense thin film. It is noteworthy that even at an extremely low driving potential (approx. 0.4 V), a distinct anodic peak appears in the CV curve of the nano-columnar porous $\text{WO}_{3-x}/\text{TiO}_2$ thin film. The charge capacity of the nano-columnar porous $\text{WO}_{3-x}/\text{TiO}_2$ thin film is over twice higher than that of the dense film. The enhancement of the injected charge capacity is absolutely attributed to the nano-columnar structure and the porous space between the nano-columns, resulting in easy ion diffusion and larger surface area for charge-transfer reactions.

Since the colored/bleached dynamics are limited by the diffusing ions, the fundamental intercalation or deintercalation diffusion coefficient of the Li^+ ions needs to be studied to establish links between the detailed kinetic behavior and electrochromic properties. Fig. 5 shows the CV curves of the two films at the applied potential ± 1.2 V with different scan rates. The cathodic and anodic peak currents corresponding to reduction and oxidation increase with the scan rates. For the nano-columnar porous thin film, the intensities of the cathodic peak current are equivalent to the intensities of the anodic peak current, indicating a good reversibility of the thin film.

The cathodic and anodic peak current values are plotted as a function of the square root of the scan rates, as shown in Fig. 6. A straight line is obtained for each thin film after linear simulation ($R > 0.99$). Based on the Randles-Sevcik equation^[23], the slope of the line can be expressed by Eq.(1):

$$K = 2.69 \times 10^5 An^{\frac{3}{2}} D^{\frac{1}{2}} C_0 \quad (1)$$

where K is the slope of the line; effective area of thin film A is 4 cm^2 ; electron number n is assumed to be 1; active ion concentration C_0 is $1 \times 10^{-3} \text{mol}\cdot\text{cm}^{-3}$; D is the ion diffusion coefficient ($\text{cm}^2\cdot\text{s}^{-1}$).

Table 1 lists the calculated ion intercalation/deintercalation diffusion coefficients. Both the ion intercalation diffusion rate and deintercalation diffusion rate of the nano-columnar porous thin film are faster than those of the dense thin film. In particular, the ion deintercalation diffusion rate is an order of magnitude faster. The results suggest that the nano-columnar porous thin film possesses good ion transport capabilities. Open-pore voids between the nano-columns decrease the Li^+ ion diffusion path length. Furthermore, vertically aligned nano-columns have good contact with both the ITO substrate and the electrolyte. Therefore, vertically aligned nano-columns provide a large active surface area available for electrochemical reactions and fast charge transport, which allows a sufficient number of Li^+ ions to intercalate into the $\text{WO}_{3-x}/\text{TiO}_2$ thin film. A fast response speed (colored/bleached within 10 s) is achieved.

To evaluate the electrochromic cyclic stability, CV curves of dense and nano-columnar porous $\text{WO}_{3-x}/\text{TiO}_2$ thin films were measured 500 times at the applied potential of ± 1.2 V

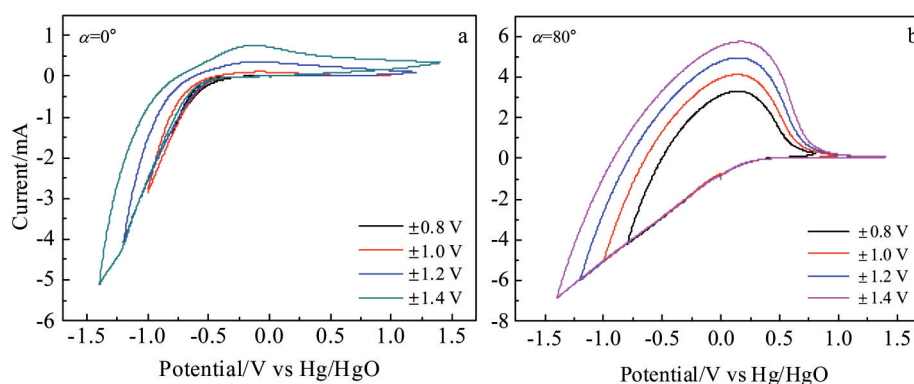


Fig.4 CV curves obtained at scan rate of 50 mV/s under different applied potentials for $\text{WO}_{3-x}/\text{TiO}_2$ films deposited at glancing angles of 0° (a) and 80° (b)

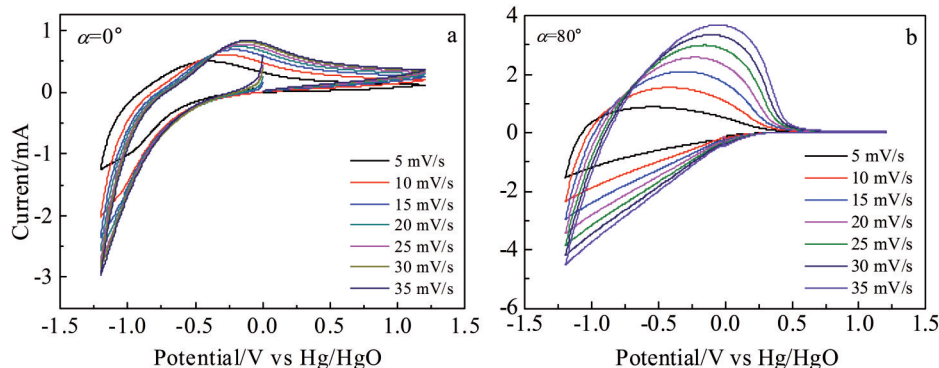


Fig.5 CV curves obtained at different scan rates under applied potential ±1.2 V for WO_{3-x}/TiO₂ thin films deposited at glancing angles of 0° (a) and 80° (b)

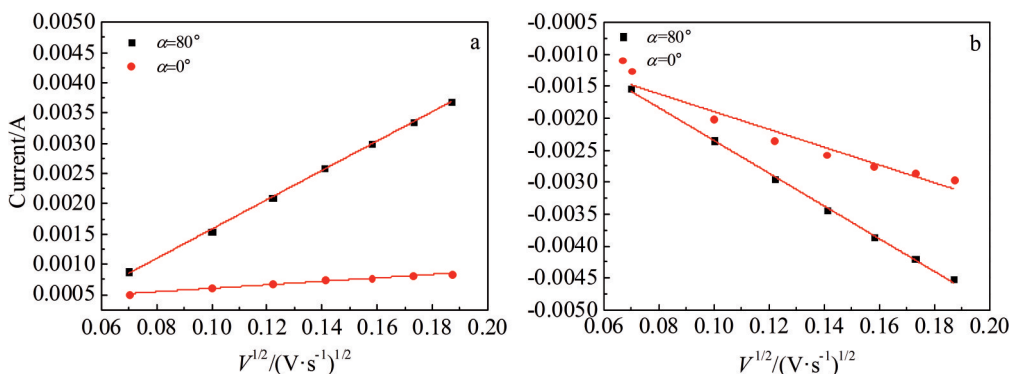


Fig.6 Cathodic (a) and anodic (b) peak current values plotted against square root of scan rate for WO_{3-x}/TiO₂ thin films deposited at glancing angles α=0° and α=80°

Table 1 Ion intercalation/deintercalation diffusion coefficient of WO_{3-x}/TiO₂ thin films (cm²·s⁻¹)

Glancing angle	Ion diffusion coefficient/×10 ⁻¹⁰	
	D _{in}	D _{dc}
α=0°	1.45	0.21
α=80°	5.69	5.08

with the scan rate of 50 mV·s⁻¹ (Fig. 7). Compared with the dense film, the cathodic peak current as well as anodic peak

current of the nano-columnar porous WO_{3-x}/TiO₂ thin film are higher, near to 4 mA. As a result, the charge capacities of nano-columnar porous WO_{3-x}/TiO₂ thin film almost double that of dense film, which is attributed to the porous structure offering more transport paths. The charge capacities of the dense film decrease rapidly from 30.83 mC to 23.02 mC during the first 100 cycles, and then it tends to be stable at about 21.5 mC from 100 cycles to 500 cycles. For the nano-columnar porous WO_{3-x}/TiO₂ thin film, the anodic current value 2.63 mA after 500 cycles is approximately decreased by 22.4% compared with 3.39 mA after 100 cycles. The charge

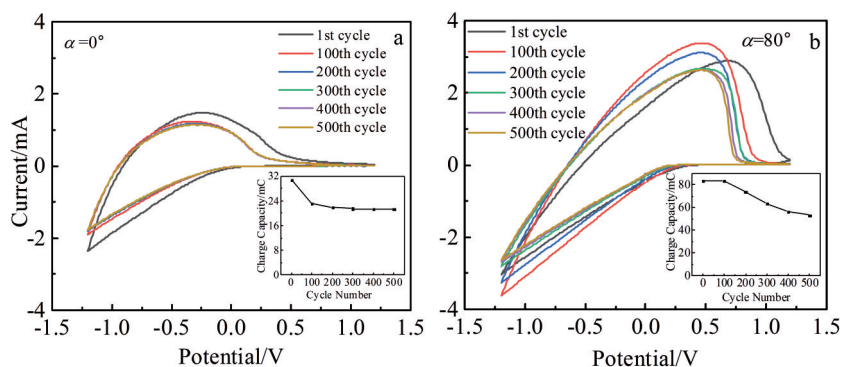


Fig.7 CV curves of WO_{3-x}/TiO₂ film deposited at glancing angles α=0° (a) and α=80° (b) in 1 mol/L LiClO₄/PC solution with scan rate of 50 mV·s⁻¹ from -1.2 V to 1.2 V

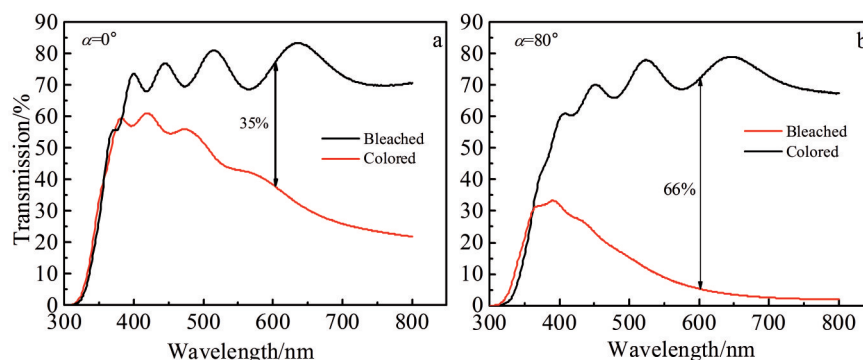


Fig.8 Transmittance spectra of colored/bleached states of $\text{WO}_{3-x}/\text{TiO}_2$ thin film deposited at glancing angles $\alpha=0^\circ$ (a) and $\alpha=80^\circ$ (b)

capacities of the nano-columnar porous $\text{WO}_{3-x}/\text{TiO}_2$ thin film are gradually declined from 83.35 mC to 53.27 mC within 100~500 cycles. It seems that the nano-columnar porous $\text{WO}_{3-x}/\text{TiO}_2$ thin film is unstable compared with the dense film. However, the current values and charge capacities of nano-columnar porous $\text{WO}_{3-x}/\text{TiO}_2$ thin film are still much larger than those of dense film after 500 cycles. Furthermore, it is better than nano-structured pure WO_3 thin film, which was studied in our previous work^[16,17]. The result suggests that the presence of surface TiO_2 reduces the ion injection/extraction diffusion rate, while it offers better colored/bleached cyclic stability under the driving potential range of ± 1.2 V, which means that TiO_2 can effectively inhibit the performance degradation of pure WO_3 thin film and protect its surface.

2.3 Thin films transmittance properties

The transmittance spectra are important means to evaluate the electrochromic performance of the thin films in the colored/bleached states, so the transmittance spectra of the $\text{WO}_{3-x}/\text{TiO}_2$ thin films in colored/bleached states are shown in Fig.8. The transmittance of colored $\text{WO}_{3-x}/\text{TiO}_2$ thin film with nano-columnar porous structure is lower than 30% in the whole visible wavelength, and even 10% as the wavelengths shift to 550 nm, suggesting that a large number of ions must insert into the film. The light modulation amplitude of nano-columnar porous film reaches 66% at a wavelength of 600 nm, much larger than that 35% of the dense film. Enhanced light modulation amplitude is attributed to nano-columnar

porous structure promoting Li^+ ions and electrons sufficiently to intercalate or deintercalate. After colored $\text{WO}_{3-x}/\text{TiO}_2$ thin films are oxidized, both films are completely reversed to their initial states. The transmittance of thin films is recovered to approximately 75%, which demonstrates better reversibility.

The transmittance modulation ability in the visible wavelength range is further evaluated by optical density variation (ΔOD), as shown in Fig.9. The ΔOD of the nano-columnar $\text{WO}_{3-x}/\text{TiO}_2$ film is better than that of the dense thin film, which suggests that the optical modulation ability of nano-columnar porous thin film is good.

3 Conclusions

1) Nano-columnar porous structure $\text{WO}_{3-x}/\text{TiO}_2$ thin film deposited by magnetron sputtering at glancing angle $\alpha=80^\circ$ displays good electrochromic properties. Compared with the dense thin film, the nano-columnar porous film is colored to dark blue at a relative low driving potential, suggesting its high sensitivity.

2) The intercalation/deintercalation ion diffusion rates of nano-columnar porous film are $D_{\text{in}}=5.69 \times 10^{-10} \text{ cm}^2 \cdot \text{s}^{-1}$ and $D_{\text{de}}=5.08 \times 10^{-10} \text{ cm}^2 \cdot \text{s}^{-1}$, respectively, which are faster than $D_{\text{in}}=1.45 \times 10^{-10} \text{ cm}^2 \cdot \text{s}^{-1}$ and $D_{\text{de}}=2.10 \times 10^{-11} \text{ cm}^2 \cdot \text{s}^{-1}$ for the dense film. The porous nano-columns facilitate the ion injection and extraction by shortening the ionic diffusion path length.

3) The electrochromic cyclic stability of nano-columnar porous $\text{WO}_{3-x}/\text{TiO}_2$ thin film is better than that of pure WO_3 thin film, indicating that presence of TiO_2 can effectively inhibit the performance degradation and protect its surface.

4) In respect of optical properties, the light modulation amplitude of nano-columnar porous film reaches 66% at 600 nm, which is larger than that of the dense film. Therefore, nano-columnar porous $\text{WO}_{3-x}/\text{TiO}_2$ thin film might be applied to fabricate the electrochromic devices with highly enhanced electrochromic properties.

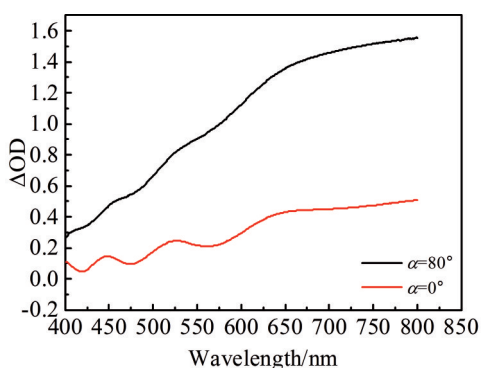


Fig.9 Optical density variation (ΔOD) of $\text{WO}_{3-x}/\text{TiO}_2$ thin films deposited at glancing angles $\alpha=0^\circ$ and $\alpha=80^\circ$

References

- 1 Zhang Jinwei, Diao Xungang, Ma Rong et al. *Rare Metal Materials and Engineering* [J], 2008, 37(9): 1688 (in Chinese)
- 2 Blanchard F, Baloukas B, Martinu L. *Applied Materials Today* [J], 2018, 12: 235

- 3 Thummavichai K, Trimby L, Wang N et al. *Journal of Physical Chemistry C*[J], 2017, 121: 20 498
- 4 Wang M, Lei H, Wen J et al. *Applied Surface Science*[J], 2015, 359: 521
- 5 Fan Yun, Tang Wu, Weng Xiaolong et al. *Rare Metal Materials and Engineering* [J], 2009, 38(9): 1570 (in Chinese)
- 6 Göttsche J, Hinsch A, Wittwer V. *Solar Energy Materials and Solar Cells*[J], 1993, 31(3): 415
- 7 Wang Z, Hu X. *Electrochim Acta*[J], 2001, 46(13-14): 1951
- 8 Hashimoto S, Matsuoka H. *Journal of the Electrochemical Society*[J], 1991, 138(8): 2403
- 9 Patil P S, Mujawar S H, Inamdar A et al. *Applied Surface Science* [J], 2005, 252(5): 1643
- 10 Reyes-Gil K R, Stephens Z D, Stavila V et al. *ACS Applied Materials & Interfaces*[J], 2015, 7(4): 2202
- 11 Gui Y, Blackwood D J. *Journal of the Electrochemical Society* [J], 2015, 162(10): 205
- 12 Pal B, Vijayan B L, Krishnan S G et al. *Journal of Alloys and Compounds*[J], 2018, 740: 703
- 13 Liu K I, Hsueh Y C, Su C Y et al. *International Journal of Hydrogen Energy*[J], 2013, 38(19): 7750
- 14 Limnonthakul P, Luangtip W, Puttharugsa C et al. *Materials Today: Proceedings*[J], 2017, 4(5): 6218
- 15 Gil-Rostra J, García-García F J, Ferrer F J et al. *Thin Solid Films* [J], 2015, 591: 330
- 16 Wang Meihan, Wen Jiaying, Chen Yun et al. *Journal of Inorganic Materials*[J], 2018, 33(12): 1303 (in Chinese)
- 17 Wang M, Chen Y, Gao B et al. *Advanced Electronic Materials* [J], 2019, 5(5): 1 800 713
- 18 Rydosz A, Dyndal K, Kollbek K et al. *Vacuum*[J], 2020, 177: 109 378
- 19 Barranco A, Borrás A, Gonzalez-Elipe A R et al. *Progress in Materials Science*[J], 2016, 76: 59
- 20 Charles C, Martin N, Devel M et al. *Thin Solid Films*[J], 2013, 534: 275
- 21 Cantalini C, Wlodarski W, Li Y et al. *Sensors and Actuators B: Chemical*[J], 2000, 64: 182
- 22 Vargas M, Lopez D M, Murphy N R et al. *Applied Surface Science*[J], 2015, 353: 728
- 23 Shiyonovskaya I, Hepel M, Tewksbury E. *Journal of New Materials for Electrochemical Systems*[J], 2000, 3(3): 241

纳米柱状多孔 $\text{WO}_{3-x}/\text{TiO}_2$ 薄膜的电致变色性能

王美涵¹, 陈 昀¹, 王冠杰¹, 雷 浩², 孙立贤³, 徐 芬³, 张 钧¹

(1. 沈阳大学 机械工程学院, 辽宁 沈阳 110044)

(2. 铝谷产业技术研究院, 山东 邹平 256200)

(3. 桂林电子科技大学 广西信息材料重点实验室, 广西 桂林 541004)

摘要: 采用反应磁控溅射在掠射角度 $\alpha=0^\circ$ 和 $\alpha=80^\circ$ 的条件下制备氧化钨 (WO_{3-x}) 薄膜, 然后在其表面沉积二氧化钛 (TiO_2)。利用 X 射线衍射仪 (XRD)、场发射扫描电镜 (FE-SEM) 和 X 射线光电子能谱仪 (XPS) 对 $\text{WO}_{3-x}/\text{TiO}_2$ 薄膜的晶体结构、表面/断面形貌以及表面化学成分进行表征。在三电极体系 1 mol/L LiClO_4/PC 溶液中, 采用电化学工作站和紫外-可见分光光度计测试了 $\text{WO}_{3-x}/\text{TiO}_2$ 薄膜的电致变色性能。XRD 结果表明, $\text{WO}_{3-x}/\text{TiO}_2$ 薄膜为非晶态结构, 与掠射角度无关。当掠射角度为 80° 时, 获得了纳米柱状多孔薄膜。从 W 4f 和 Ti 2p 的 XPS 谱图确认氧化钨为亚化学计量比的 WO_{3-x} , 而氧化钛为满足化学计量比的 TiO_2 。与致密薄膜相比, 纳米柱状多孔薄膜需要较低的驱动电压且具有较快的响应速度。纳米柱状多孔薄膜的电荷容量为 83.78 mC, 是致密薄膜电荷容量 30.83 mC 的 2 倍以上。在 ± 1.2 V 驱动电压下, 注入和脱出离子扩散速率分别为 $D_{\text{in}}=5.69 \times 10^{-10} \text{ cm}^2/\text{s}$ 和 $D_{\text{de}}=5.08 \times 10^{-10} \text{ cm}^2/\text{s}$ 。与纯 WO_3 薄膜相比, $\text{WO}_{3-x}/\text{TiO}_2$ 薄膜的电致变色循环稳定性更好。纳米柱状多孔薄膜在可见光范围内具有较大的光调制幅度, 因此其光密度变化 (ΔOD) 大于致密薄膜。

关键词: $\text{WO}_{3-x}/\text{TiO}_2$ 薄膜; 纳米柱状; 掠射角; 磁控溅射; 电致变色性能

作者简介: 王美涵, 女, 1977 年生, 博士, 教授, 沈阳大学机械工程学院, 辽宁 沈阳 110044, E-mail: mhwang@syu.edu.cn